

Vascular Endothelial Growth Factor Mimetic Peptide and Parathyroid Hormone (1–34) Delivered *via* a Blue-Light-Curable Hydrogel Synergistically Accelerate Bone Regeneration

Guiyan Wang,[†] Ning Yuan,[†] Ningyu Li, Qijia Wei, Yuping Qian, Jun Zhang, Man Qin, Yuguang Wang,* and Suwei Dong*



Cite This: <https://doi.org/10.1021/acsami.2c06159>



Read Online

ACCESS |



Metrics & More



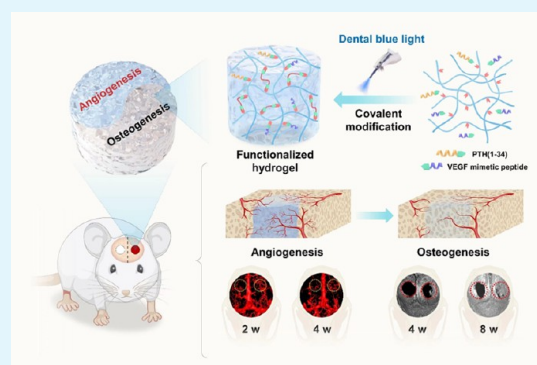
Article Recommendations



Supporting Information

ABSTRACT: Safe and effective biomaterials are in urgent clinical need for tissue regeneration and bone repair. While numerous advances have been made on hydrogels promoting osteogenesis in bone formation, co-stimulation of the angiogenic pathways in this process remains to be exploited. Here, we have developed a gelatin-based blue-light-curable hydrogel system, functionalized with an angiogenic vascular endothelial growth factor (VEGF) mimetic peptide, KLTWQELYQLKYKGI (KLT), and an osteoanabolic peptide, parathyroid hormone (PTH) 1–34. We have discovered that the covalent modification of gelatin scaffold with peptides can modulate the physical properties and biological activities of the produced hydrogels. Furthermore, we have demonstrated that those two peptides orchestrate synergistically and promote bone regeneration in a rat cranial bone defect model with remarkable efficacy. This dual-peptide-functionalized hydrogel system may serve as a promising lead to functional biomaterials in bone repair and tissue engineering.

KEYWORDS: VEGF mimetic peptide, PTH(1–34), covalent functionalization, blue-light-curable hydrogel, bone regeneration



INTRODUCTION

Large bone defects caused by trauma, tumors, and infectious diseases reduce patients' quality of life and remain a daunting challenge worldwide. Autogenous transplantation is the gold standard for bone therapy but is significantly restrained by the sources of autografts, as allografts and xenografts often encounter host rejection issues.¹ Various biomaterials developed for bone tissue engineering have shown superior clinical results,^{2–4} such as FDA-approved Medtronic's Infuse Bone Graft and Stryker's OP-1. These synthetic bone grafts utilize growth factors, including recombinant human bone morphogenetic protein 2 (rhBMP-2), and BMP-7, to promote osteoinduction.⁵ However, the applied bioactive proteins are limited to certain types, and another essential process in bone repairing, vascularization,⁶ is often overlooked in developing related biomaterials. Compared with macromolecular proteins, bioactive peptides provide great therapeutic potential owing to their short amino acid sequences, readily accessibility, and relatively low cost.⁷ Moreover, peptides can be easily modified to achieve controllable release and the modulation of various pathways involved in bone formation. Thus, the development of novel bioactive peptide-functionalized biomaterials is of promising prospect for bone tissue engineering.⁸

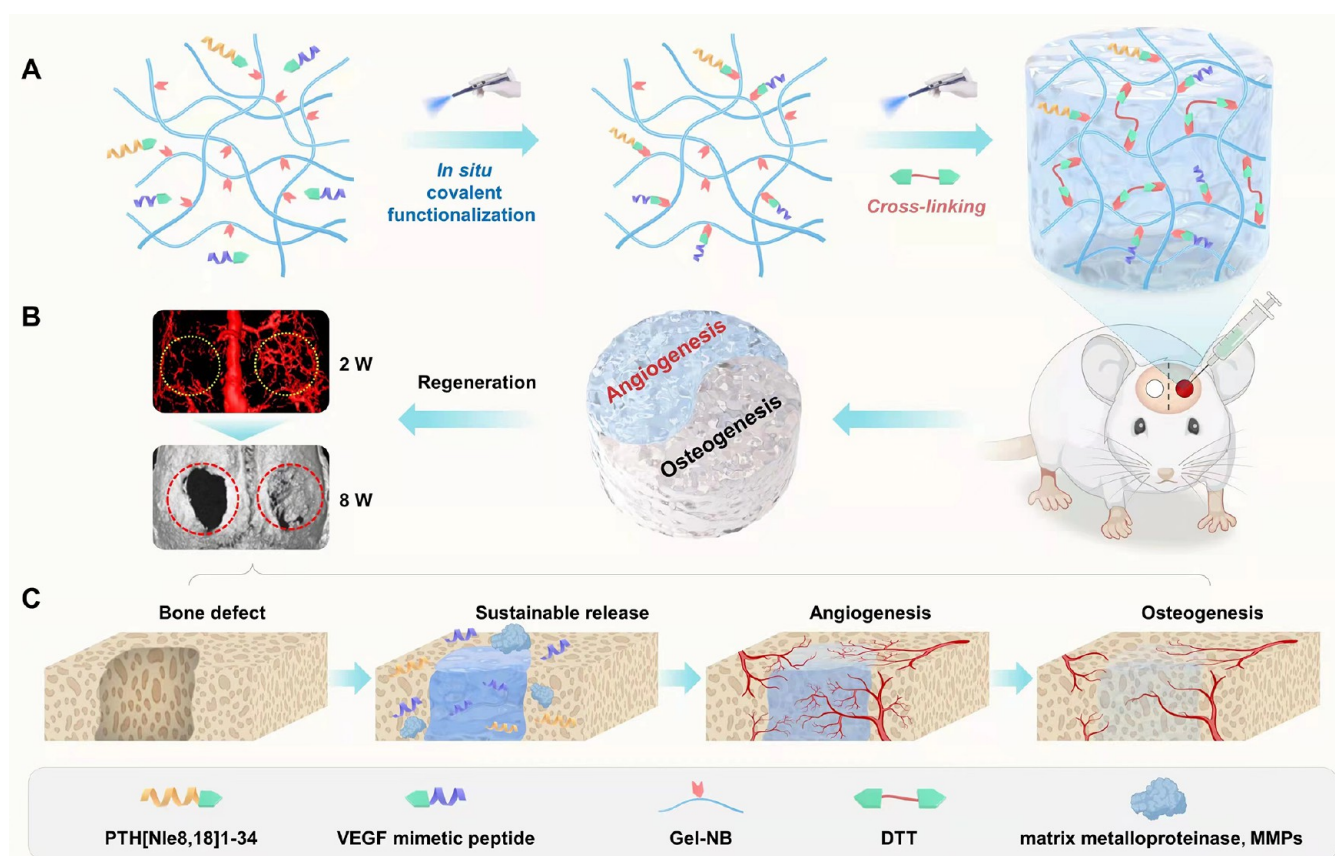
Hydrogels represent an advantageous type of scaffolds for tissue engineering that can deliver bioactive peptides with

excellent biocompatibility, viscoelasticity, and mechanical properties.^{9,10} Several studies have shown that using osteogenic peptides to functionalize hydrogels is beneficial for bone regeneration. For instance, Qiao et al. developed a gelatin-based hydrogel modified by osteogenic growth peptide (OGP) for repairing rat distal femur defects *in vivo*,¹¹ and Li et al. functionalized a hyaluronic acid (HA) hydrogel with Foxy5, a Wnt5a mimetic hexapeptide, to repair rat calvarial defects with excellent efficiency.¹² These successful examples, along with other precedents such as the hydrogel functionalized by BMP-2 mimetic peptides (BP),¹³ mainly focus on the osteogenic signaling pathways, albeit the bone regeneration process is highly complicated and affected by various factors.^{14,15} We envisaged that combining two types of peptides with different bioactivities, such as an angiogenic vascular endothelial growth factor (VEGF) mimetic peptide, KLTWQELYQLKYKGI (KLT),^{16,17} and an osteoanabolic peptide, parathyroid hormone (PTH) 1–34,¹⁸ may impact both the vascularization and osteoinduction processes, thus synergizing bone regeneration.¹⁹

Herein, we report a dental blue-light-curable hydrogel scaffold functionalized with KLT and PTH peptides, which synergistically

Received: April 8, 2022

Accepted: July 14, 2022

Scheme 1. VEGF Mimetic Peptide KLT and PTH(1–34) Delivered *via* a Dental Blue-Light-Curable Hydrogel Accelerate the Repair of Rat Cranial Defects⁴

(A) Schematic illustration of the fabrication of dual-peptide-functionalized hydrogel *via* an *in situ* covalent functionalization strategy. KLT and PTH(1–34) peptides were covalently attached to the gelatin scaffold efficiently through a rapid photoinduced thiol-norbornene click reaction. (B) The application of the KLT/PTH-functionalized hydrogel with both angiogenic and osteogenic bioactivities for rat cranial defects repairing. Top left: A representative neovascularization micro-CT image after vascular perfusion showing cranial defect angiogenesis. Bottom left: A representative micro-CT image of the cranial bone defect areas showing the bone repair. (C) Schematic illustration of the regenerative process after implantation of the KLT/PTH-functionalized hydrogel. The bioactive peptides could be slowly released upon the degradation of hydrogel scaffold by matrix metalloproteinases (MMPs), presenting a favorable microenvironment for early blood vessel growth and the followed bone reconstruction.

cally accelerated bone regeneration, presumably through promoting the blood vessel growth at the early stage, and the followed bone reconstruction processes (Scheme 1). The bioactive peptides are covalently linked to the hydrogels utilizing a photoinduced thiol-norbornene reaction, which effectively enhances the preservation of the bioactive agents.^{8,20–22} The prepared hydrogels were evaluated in cell proliferation, adhesion, and migration assays *in vitro*, and in a rat cranial defect model for their bone regeneration-promoting capacity, showing an optimal regenerative efficacy of 77% bone volume/tissue volume (BV/TV). Furthermore, the synergistic osteogenic and angiogenic effects of combining KLT and PTH(1–34) were also probed.

EXPERIMENTAL SECTION

Materials. Cold water fish gelatin, ascorbic acid, dexamethasone, *b*-glycerophosphate, and Alizarin Red S were all purchased from Sigma-Aldrich. 5-Norbornene-2-carboxylic acid, 1-ethyl-3-(3-dimethylpropylamine) carbodiimide (EDCI), *N*-hydroxysuccinimide (NHS), *N,N'*-diisopropylcarbodiimide (DIC), anhydrous dimethylsulfoxide (DMSO), deuterioxide (D₂O), and 4-methylpiperidine were purchased from Energy Chemical. All reagents for peptide synthesis including Fmoc-protected amino acids, Fmoc-rink amide MBHA resin, and

oxyma were purchased from GL Biochem (Shanghai) Ltd. HPLC-grade acetonitrile and dimethyl formamide (DMF) were purchased from Oceanpak. The CCK-8 reagents were purchased from Dojindo. The Live Green and Dead Red reagents and Actin-Tracker Green were purchased from KeyGEN. The RNA Isolation Reagents TRIzol was purchased from Invitrogen, the reverse-transcription kit was purchased from TAKARA, and the Matrigel was purchased from Corning. The α -MEM and FBS were purchased from Gibco. The BCIP/NBT ALP Assay Kit was purchased from Beyotime. The MICROFIL was purchased from the Flow Tech. H&E staining kit (Hematoxylin and Eosin) and Masson's trichrome staining kit were obtained from Solarbio Life Science. The immunohistochemistry antibodies were purchased from Abcam and Proteintech.

General Protocols for Peptide Synthesis. The peptides were prepared following the reported protocol with minor optimization.²³ Briefly, a CEM Liberty Blue system with microwave irradiation was adopted with a 0.05 mmol scale using a 5-fold excess of reagents (0.2 M amino acid solution in DMF, 0.25 M DIC in DMF, 0.5 M Oxyma in DMF), and coupling for 2 min at 90 °C (50 °C 10 min for Fmoc-Cys(Trt)-OH and Fmoc-His(Trt)-OH, 75 °C 10 min for Fmoc-Arg(Pbf)-OH). For amino acids after sterically hindered residues such as arginine, isoleucine, threonine, valine, and proline, double couplings were conducted. The Fmoc removal step was conducted using a deblock solution of 20% 4-methylpiperidine in DMF (v/v) for 30 s at 90 °C. The peptide resin was washed with DCM three times after synthesis

and treated with a solution of TFA/TIPS/H₂O (95/2.5/2.5, v/v/v) for 2 h. The resin was then removed by filtration, and the filtrate was concentrated under a nitrogen atmosphere. The resulting residue was triturated with cold diethyl ether to give a white solid, which was then dissolved in a solution of acetonitrile and water containing 5% acetic acid. The resulting solution was ready for LC–MS analysis or HPLC purification after filtration. All HPLC separations involved a mobile phase of 0.05% (v/v) TFA in water (solvent A) and 0.04% (v/v) TFA in MeCN (solvent B).

Binding Tests of PTH(1–34) Derivative Peptides. A cAMP assay was conducted to test the activities of PTH(1–34) derivative peptides. The measurement was carried out using a cAMP-Gs Dynamic kit (62AM4PEB, Cisbio) according to the manufacturer's protocol. In detail, 293T cells stably expressing PTH1R were seeded at a density of 2000 cells per well into HTRF 96-well low-volume plates (66PL96025, Cisbio), followed by incubation with PTH[Nle8,18]_{1–34}, GCG-PTH[Nle8,18]_{1–34} and PTH[Nle8,18]_{1–34}-GCG peptides for 30 min. Then, cAMP-d2 conjugate and cryptate conjugate in lysis buffer were added and incubated for another 60 min. Fluorescence data were read with Biotek Synergy Neo2, and the curve was calculated by nonlinear regression (three-parameter logistic fit) in GraphPad.

Synthesis of GelNB. The synthesis of GelNB was conducted following the reported methods with minor optimization.²⁴ Briefly, 2.00 g of 5-norbornene-2-carboxylic acid (7.20 mmol) was first dissolved in 40 mL of dichloromethane. Then, an additional 2.24 g of *N*-hydroxysuccinimide (NHS-OH, 19.46 mmol) and 3.58 g of EDCI (18.68 mmol) were added, and the mixed solution was stirred at room temperature for 24 h. The reaction mixture was poured into 100 mL of ethyl acetate and washed with 80 mL of saturated NaHCO₃ solution, twice with 80 mL of water and once with 80 mL of brine. The organic layer was collected and dried over anhydrous magnesium sulfate (MgSO₄). The dried solution was then evaporated *in vacuo* to yield a white solid product (yield: 3.41 g, *ca.* 85%), which was used without further purification for the next step.

Gelation (10.00 g, –NH₂ = 3.06 mmol) from cold water fish (Sigma-Aldrich) was dissolved in DMSO in a 50 °C water bath under argon protection, followed by the addition of the synthesized 5-norbornene-2-NHS ester (1.00 g, 4.25 mmol). The reactant solution was stirred at 50 °C in an oil bath for 24 h before addition to a tenfold volume of acetone. The suspension was filtered, and the white precipitate was washed with acetone three times and then dried under vacuum overnight. The crude gelatin was redissolved in 80 mL of deionized water and centrifuged to remove the undissolved impurity. The pH of the solution was adjusted to approximately 7.5 with 1 N NaOH solution before dialysis with deionized water for 3 days at 40 °C. Finally, the solution was collected and lyophilized to provide the product as a white solid (yield: 8.52 g, *ca.* 82%). The modified GelNB was characterized with 400 Hz NMR, and the degree of substitution (DS) was measured with an ortho-phthalic dialdehyde assay.

Dental Blue Light-Induced Gelation Tests. The gelation abilities of GelNB cross-linked with three different thiol-linkers, DTT, HS-PEG-SH (MW = 2k, Macklin), and MMP-degradable peptide linker, were investigated. First, 5, 10, and 15% GelNB solutions in 0.1 mM eosin Y in DPBS were prepared. Then, a proper amount of linker was dissolved in the prepared GelNB solutions, confirming that the amount of thiol groups on the linker was equal to the norbornene groups on the gelatin chain. After thorough mixing, 200 μ L of hydrogel precursor was transferred to a 4 mL sample vial and exposed to light-emitting diode (LED) dental blue light (LY-B200, 420–480 nm, 1200–2000 mW/cm²) at a 5 mm distance and checked every 5 s. The gelation was confirmed by inversion of the vial, and the gelation time points were recorded.

General Procedure for Hydrogel Preparation. Gel-NB (75.00 mg) dissolved in 468.75 μ L of 0.1 mM Eosin Y solution with or without thiol-modified peptides was used to prepare a 16% Gel-NB solution. Then, 56.00 mg of DTT was dissolved in 1.00 mL of 0.1 mM eosin Y solution to provide DTT thiol-linker solution. To the above 468.75 μ L of 16% Gel-NB solution, 31.25 μ L of DTT thiol-linker solution was added and mixed thoroughly, after which the hydrogel precursor was transferred to a Teflon cuboid mold (length = width = 10 mm, height =

5 mm) and exposed to dental blue light to form a hydrogel. Hydrogels were prepared following this protocol for compression, *in vitro* swelling and degradation, rheological tests, and scanning electron microscopy (SEM) analysis.

Peptide Covalent Functionalization and Release Test. Thiol-containing peptide was dissolved in 0.1 mM eosin Y, followed by the dissolution of GelNB. The prepared solution was exposed to dental blue light for 5 min for covalent prefunctionalization, and then DTT thiol-linker solution in 0.1 mM eosin Y was added. The solution was mixed thoroughly before addition to the mold and light exposure to form a hydrogel.

Peptide release tests were conducted with Alliance e2695 analytic HPLC equipped with an Agilent C18 column (Eclipse XDB-C18, 5 μ m, 4.6 mm \times 150 mm). Briefly, a calibration curve of the test peptide with certain concentrations (i.e., 10, 25, 50, 75, 100, 150 μ g/mL) was established according to the peak area integration. Then, 500 μ L of cuboid hydrogels (length = width = 10 mm, height = 5 mm) of 15% GelNB containing covalently or noncovalently immobilized peptides was prepared. The hydrogels were incubated in centrifugal tubes with 2 mL of DPBS at 37 °C. After this, 1 mL of the solution was taken from each tube at different time points (i.e., 30 min, 60 min, 12 h, 1 day, 2 days, 3 days, etc.), after which 1 mL of DPBS was added. The aliquots were analyzed with HPLC, and the concentration of the peptides was calculated according to the calibration curve.

Physical Characterizations of Peptide-Functionalized Hydrogels. Four groups of 500 μ L cuboid hydrogels (length = width = 10 mm, height = 5 mm) composed of 15% GelNB covalently functionalized without peptides, with 1 mg/mL PTH[Nle8,18]_{1–34}-GCG, 5 mg/mL GCG-KLT, 1 mg/mL PTH[Nle8,18]_{1–34}-GCG, and 5 mg/mL GCG-KLT, were prepared and used in the following tests.

Compression tests were conducted using an Instron 5696 mechanical tester at a rate of 5 mm/min until failure. Compressive strain (mm) and load (*N*) were then measured using Instron's Bluehill 3 software. Moduli were determined by obtaining the tangent of the slope of the linear region on the loading stress/strain curve between 25 and 35% (*n* = 5).

The adhesive tests were conducted with porcine skin. The hydrogel (50 μ L) was photo-cross-linked with two pieces of porcine skin (10 mm \times 10 mm). The adhesive strength was measured with an Instron 5696 mechanical tester at a speed of 5 mm/min until two pieces of porcine skin separated (*n* = 5).

The porosity of the cross-linked hydrogels was evaluated with SEM imaging and analysis. Lyophilized hydrogel samples were prepared first. SEM images were obtained using a scanning electron microscope (Zeiss Merlin FE-SEM). Pore sizes of the hydrogels were averaged from at least three images from three samples for each condition (*n* = 5).

Swellability of the hydrogels was determined by incubating the hydrogels in DPBS at 37 °C for 24 h. Hydrogels were prepared and lyophilized, and their dried weights were measured (W_{dry}). At specific time points of 30 min, 1 h, 2 h, 4 h, 8 h, 12 h, and 24 h, hydrogels were then removed from the buffer and weighed to obtain swollen weights ($W_{swollen}$). Swelling ratio was calculated by $W_{swollen}/W_{dry}$ (*n* = 4).

To evaluate the degree of *in vitro* degradation, hydrogels were lyophilized and weighed to record the initial weights (W_0). The samples were placed in centrifugal tubes, 2 mL of collagenase II solution (5 μ g/mL in PBS) was added, followed by incubation at 37 °C. At 12 h, 24 h, 36 h, 2 days, 3 days, and 5 days, the buffer was removed and washed with DPBS 3 times for 5 min each. The samples were lyophilized and weighed (W_T). Weight loss was calculated by $W_0 - W_T/W_0$ (*n* = 4).

Rheological measurements were performed on a MARS rheometer (HAAKE). For *in situ* light-triggered oscillatory time sweep test, an external LED dental blue light as a light source with a glass plate rotor (20 mm diameter, 0.5 mm gap) was used, where all samples were measured at 10% strain and 1 Hz for 200 s and blue light was emitted from the 30th second. Every time, 100 μ L of hydrogel precursor was added to the plate and measured at 25 °C (*n* = 5). Cylinder hydrogels (*d* = 8 mm, *z* = 1 mm) were prepared for the oscillatory time sweep test with a cone rotor (35 mm diameter, 1° cone angle, 0.5 mm gap). All samples were measured at 10% strain and 1 Hz for 60 s at 25 °C (*n* = 5).

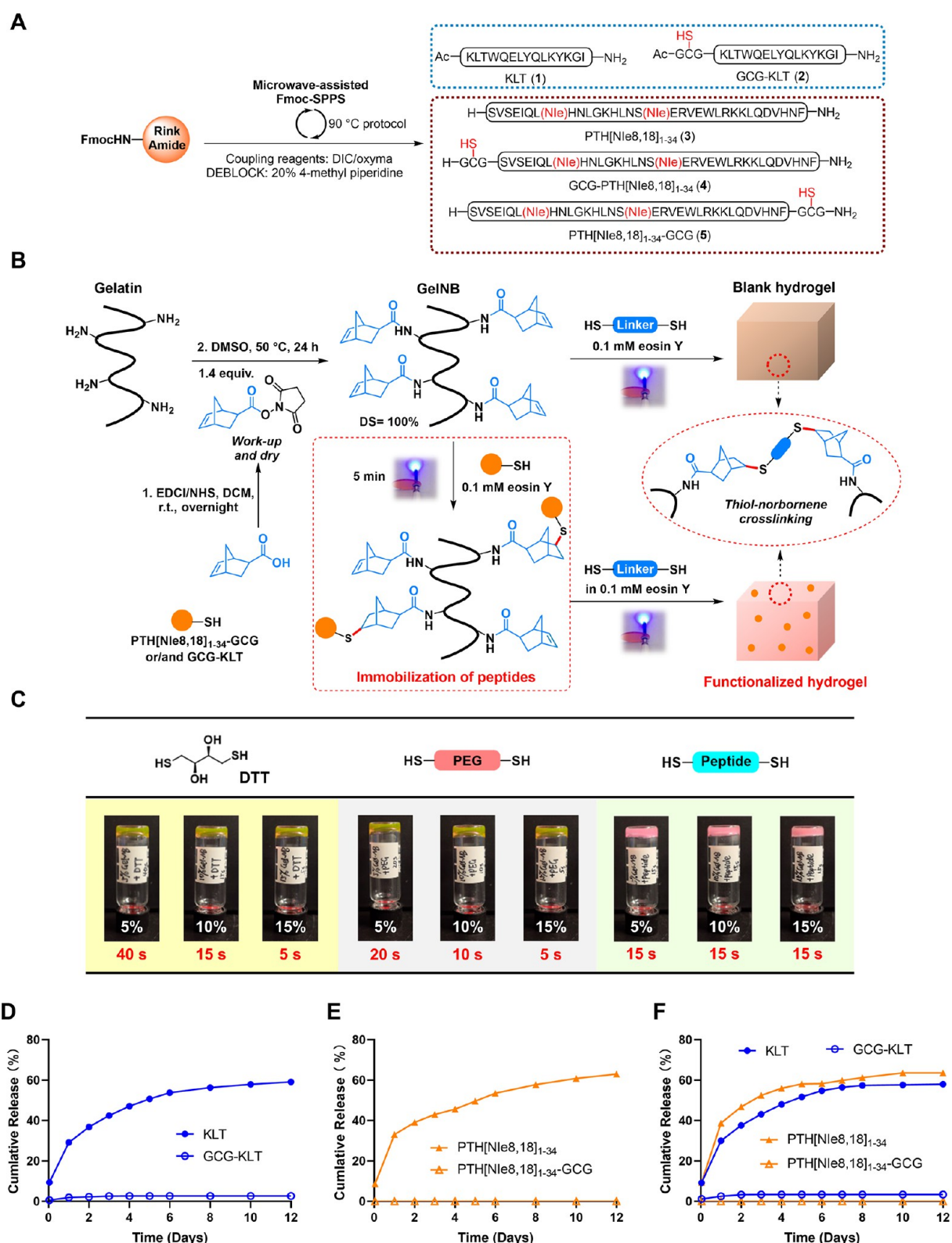


Figure 1. Fabrication of gelatin-based hydrogel covalently functionalized with KLT/PTH peptides. (A) Synthetic scheme for PTH(1–34) and KLT peptide analogues. (B) Reaction scheme for GelNB preparation, gelation tests in 0.1 mM eosin Y with dental blue light (430–480 nm) and *in situ* covalent functionalization of thiol-modified peptide into GelNB hydrogel. (C) Blue-light-induced hydrogel formation cross-linked by thiol-containing DTT, PEG, and peptide linkers in 0.1 mM eosin Y. *In vitro* release profile of noncovalently and covalently immobilized peptides from 15% (w/v) GelNB hydrogels with (D) 5 mg/mL KLT and 5 mg/mL GCG-KLT, (E) 1 mg/mL PTH[Nle8,18]₁₋₃₄ and 1 mg/mL PTH[Nle8,18]₁₋₃₄-GCG, and (F) 5 mg/mL KLT + 1 mg/mL PTH[Nle8,18]₁₋₃₄ and 5 mg/mL GCG-KLT + 1 mg/mL PTH[Nle8,18]₁₋₃₄-GCG ($n \geq 3$).

Real-Time Polymerase Chain Reaction (RT-PCR) Assay. HUVECs were cultured with PTH, KLT, or PTH/KLT medium.

After 7 days, the cells were harvested and total RNA was extracted with TRIzol (Invitrogen). The RNA concentration and quality were

measured with a NanoDrop-8000 spectrophotometer (Thermo Fisher). cDNA synthesis was performed using a reverse-transcription kit (TAKARA, Shiga, Japan). The mRNA expression of VEGF, PECAW, and vWF was measured with RT-PCR. The endogenous control to normalize the gene expression used the β -actin gene. The primers used in the present study are shown in [Supplementary Table 1](#).

HUVEC Tube Formation Assay. Briefly, 200 μ L of cold Matrigel (Corning, NY) was coated on a 24-well plate and then placed in a 37 °C incubator for 30 min to let the Matrigel cure. Then, 1×10^4 HUVECs in 500 μ L of medium were seeded on Matrigel. Additional PTH, KLT, and PTH/KLT peptide were added to the medium. After 8 hours, the images were captured with a light microscope. The number of branch points was used to evaluate the peptide ability to form capillary-like structures in three randomly chosen fields.

Chick Embryo Chorioallantoic Membrane (CAM) Assay. First, the fertilized chicken eggs were incubated at 37 °C with 80% humidity. On day 5, the embryo developed and a small window in the shell on the embryo allantoic sac was created. The medium containing PTH, KLT, or PTH/KLT was incubated with the CAMs. On day 10, the blood vessels in the incubated area were fixed and photographed with a stereomicroscope (Olympus, Japan). The number of blood vessels was quantified and calculated. In each group, 6 viable embryos were used.

Osteogenic Differentiation Tests for the PTH and KLT Peptides. Osteogenic differentiation was induced using osteogenic medium (50 mg/mL ascorbic acid, 100 nM dexamethasone, and 5 mM *b*-glycerophosphate; Sigma-Aldrich; DMEM, 10% FBS). PTH, KLT, or PTH/KLT were added to the osteogenic medium, whereas cells in the control group were cultured in an osteogenic medium. The effect of early osteogenic differentiation was evaluated by alkaline phosphatase (ALP) staining, ALP activity, and RT-PCR on day 7. On day 14, Alizarin red S staining and RT-PCR were used to assess the later osteogenic differentiation ability. For ALP staining, the cells were washed with PBS three times and fixed with 4% paraformaldehyde for 30 min. The cells were then incubated with a BCIP/NBT ALP Assay Kit (Beyotime, Shanghai, China) for 10 min. To measure the ALP activity, the protein was collected and reacted with *p*-nitrophenyl phosphate for 30 min, and then the absorbance was detected at 405 nm to measure the ALP activity. After osteogenic differentiation for 14 days, the cells were fixed for 30 min and then stained with 1% Alizarin Red S (Sigma-Aldrich) solution. To quantify mineralization, the stained cells were desorbed with 10% cetylpyridinium chloride.

Cranial Bone Defect Surgical Procedure. Before the animal experiment, the procedures were allowed by the Biomedical Ethics Committee of Peking University (LA2021106, China). Sprague-Dawley (SD) rats were provided by Beijing Charles River Laboratories. In the present study, 60 SD rats aged 6–8 weeks and weighing approximately 200 g were used. There were four experimental groups, and each group consisted of 3 SD rats. The detailed groups were as follows: (1) blank group, (2) PTH group, (3) KLT group, and (4) PTH/KLT group. Each SD rat on the left side served as the control group without hydrogel. After general anesthesia, a longitudinal incision was made in the calvarial bone, and the periosteum on the skull bone was resected. A 5 mm trephine was used to create two craniotomy defects along the middle cranial suture, with 0.9% saline continuously irrigated during the procedure. After hemostasis, the hydrogel or covalent with PTH/KLT was injected into the defects and irradiated with LED curing light (420–480 nm, 1200–2000 mW/cm²) for 2 min. The wound was sutured with 5-0 braided absorbable sutures. After the surgery, SD rats were intramuscularly injected with gentamicin sulfate (40 mg). After 4 and 8 weeks, the rats were euthanized with carbon dioxide and the calvaria were anatomically sampled. The rat skulls were preserved in 10% formalin solution for 3 days before the next experiment.

Vascular Perfusion. To evaluate blood vessel formation in skull defects, vascular perfusion was performed. Briefly, 2, 4, and 8 weeks after surgery, the rats were anesthetized, the chest was opened, and the heart was exposed. Next, the heart was perfused with heparin saline, 4% paraformaldehyde, and 20 mL of MICROFIL (Flow Tech, Carver, MA). Then, the rats were preserved overnight at 4 °C. The skulls were

harvested the next day. After decalcification, the skull was scanned to observe cranial defect angiogenesis.

Micro-CT Analysis. After fixation in 10% formalin, the skulls were scanned *via* micro-CT (GANTRY-STD CT 3121, Germany). The specific scan parameters were as follows: 80 kV, 500 μ A, 33.658 μ m pixel size, 101.800 mm source-to-center distance, and 10.590° fan beam angle. The analysis software was Inveon, and the measurement of the new bone was calculated with the bone mineral density (BMD) and BV/TV index. At the same time, the three-dimensional (3D) image was captured.

Masson, HE, and Immunohistochemistry (IHC) Analysis. After micro-CT scanning, the skulls were decalcified in 10% ethylenediaminetetraacetic acid and changed every day. The decalcified period lasted 4 weeks. Subsequently, the skull bones were embedded in paraffin, and the paraffin blocks were sectioned into 5 μ m sections. Then, the slides were stained with HE and Masson's trichrome. At the same time, the slides were detected with mouse monoclonal antibodies against platelet endothelial cell adhesion molecule-1 (PECAM-1/CD31) (Abcam) and osteocalcin (OCN) (Proteintech).

Statistical Analysis. The data are presented as the average \pm standard deviation (SD). One-way analysis of variance (ANOVA) with LSD multiple comparison tests was conducted using the Statistical Package for the Social Sciences version 20.0 (IBM Corp.). A *P* value less than 0.05 was accepted as statistically significant.

RESULTS AND DISCUSSION

Fabrication of the Peptide-Functionalized Blue-Light-Curable Hydrogel. We selected norbornene-modified gelatin (GelNB) as the hydrogel scaffold, as thiol–ene click reactions proceed efficiently under light irradiation,²⁵ allowing for a high degree of substitution (DS) preferred for the requirement of installing both cross-linkers and the bioactive peptides. Accordingly, incorporating cysteines in the peptide sequences is required but shall not compromise their biological activities. Previous studies on self-assembling peptide hydrogels have demonstrated that modification at the N-terminus of KLT peptide shows insignificant effects on its interaction with VEGF receptor,^{26,27} while the proper sites for installing cysteines in PTH(1–34) remain to be confirmed.^{28–30} With these considerations in mind, three cysteine-containing peptides were prepared using solid-phase peptide synthesis (SPPS) with a previously optimized protocol (Figure 1A),²³ including N-terminus-modified KLT (1), N-terminus-modified PTH (4), and C-terminus-modified PTH (5), along with two controlled-group sequences KLT (2) and [Nle8,18]PTH(1–34) (3). Notably, The Met residues at sites 8 and 18 in PTH were mutated to norleucine (Nle), which could increase the stability and the synthetic efficiency, but not influence the bioactivity.³¹ In a cAMP activation assay, revealing the binding ability of PTH to PTHR,³² peptide 5 exhibited similar activity to that of the unmodified peptide 3, while the N-terminal modification significantly decreased the activity leading to a much higher EC₅₀ value (Figure S1). These results were in accordance with the action mechanism of PTH, as its N-terminus is the critical region that binds to PTHR.³³ Therefore, PTH analogue 5 was chosen for further investigation.

For introducing the norbornene groups, using 1.4 equiv of preformed 5-norbornene-2-NHS ester was found to be optimal (Figure 1B),^{24,34} affording GelNB with a 100% degree of substitution (DS), as confirmed by an ortho-phthalic dialdehyde assay and ¹H NMR (Figure S2). This optimized method allows for the highest reported DS of GelNB with minimal substrate consumption and easy purification.²⁵ With the safety concerns of UV irradiated conditions in mind,^{35–37} we investigated blue light-induced gelation conditions on crosslinking GelNB with

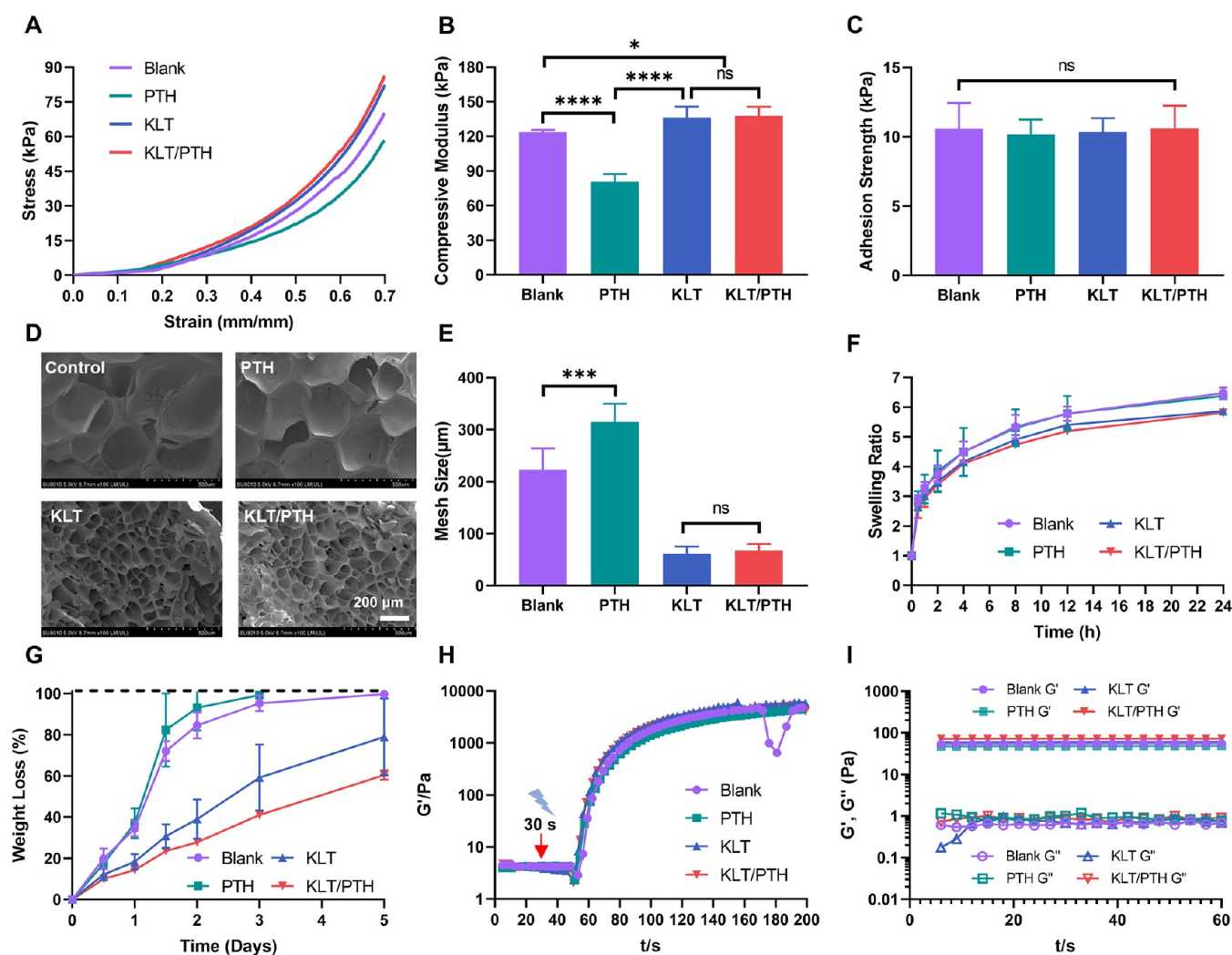


Figure 2. Physical characterization of the peptide covalently immobilized hydrogels. Four groups of GelNB hydrogels cross-linked with DTT in 0.1 mM eosin Y without peptide or covalently immobilized with 5 mg/mL KLT, 1 mg/mL PTH, and 5 mg/mL KLT + 1 mg/mL PTH were used for the following characterizations. The results from compression tests including (A) representative compressive stress–strain curves and (B) compressive modulus. (C) *In vitro* adhesion strength of the hydrogels determined with an Instron 5696 mechanical tester. (D) Representative SEM images (scale bar = 200 μm) and (E) pore size characterization. (F) Swelling ratio changes within 24 h incubation in DPBS at 37 °C. (G) *In vitro* degradation properties in 5 μg/mL collagenase type II solution in PBS. (H) *In situ* photorheometry test of hydrogel gelation kinetics. Light was placed 30 mm away from the gels, and turned on at 30 s (red arrow) after initiating the measurement. (I) Elastic modulus (G') and viscous modulus (G'') of the hydrogels measured by oscillatory time sweep tests. Data are represented as mean \pm SD (* p < 0.05, ** p < 0.01, *** p < 0.001, **** p < 0.0001, $n \geq 3$).

dithiothreitol (DTT).³⁸ Hydrogel formation proceeded rapidly under the sensitization of eosin Y (0.1 mM) with a GelNB concentration as low as 5% (Figure S3), which was much faster than the previously reported 2 min gelation time using lithium phenyl-2,4,6-trimethylbenzoyl phosphinate (LAP) as the photoinitiator.³⁹ The gelation time could be further shortened by increasing the concentration of GelNB (Figure 1C). Considering that different linkers may affect the gelation time, physical properties, and biological activities,⁴⁰ we further tested dithiol-containing poly(ethylene glycol) (PEG) and an MMP-degradable peptide linker. At the same concentration of GelNB, the PEG linker resulted in faster gelation than the DTT linker, which might be caused by the intertwining of flexible PEG chains and gelatin after the chemical crosslinking. Interestingly, the gelation rates of GelNB seemed to be independent of the concentration when using peptide as the linker, where the gelation time was approximately 15 s at each of the three concentrations. Overall, the eosin Y-promoted photo-

irradiation conditions were highly efficient and robust in producing GelNB hydrogels.^{41,42}

Next, we evaluated the efficiency for covalently immobilizing the bioactive peptides. The KLT or PTH derivative was installed onto GelNB under the blue light irradiation for 5 min, followed by the addition of a dithiol cross-linker (Figure 1B). The obtained hydrogel was incubated in Dulbecco's phosphate-buffered saline (DPBS), and the leakage of loaded peptides was monitored using high-performance liquid chromatography (HPLC). The release of the covalently linked GCG-KLT was only 2.7% after 12 days, while a significant leakage of the peptide was observed for the hydrogel prepared with noncovalently loaded KLT (Figure 1D). These results suggested that the covalent functionalization strategy can largely preserve the bioactive peptides for a slow-release under suitable stimuli (e.g., enzymatic degradations), which would be more advantageous for cases requiring slow-release as the bone regeneration may last up to 6–8 weeks. Tests using PTH peptides (Figure 1E) and

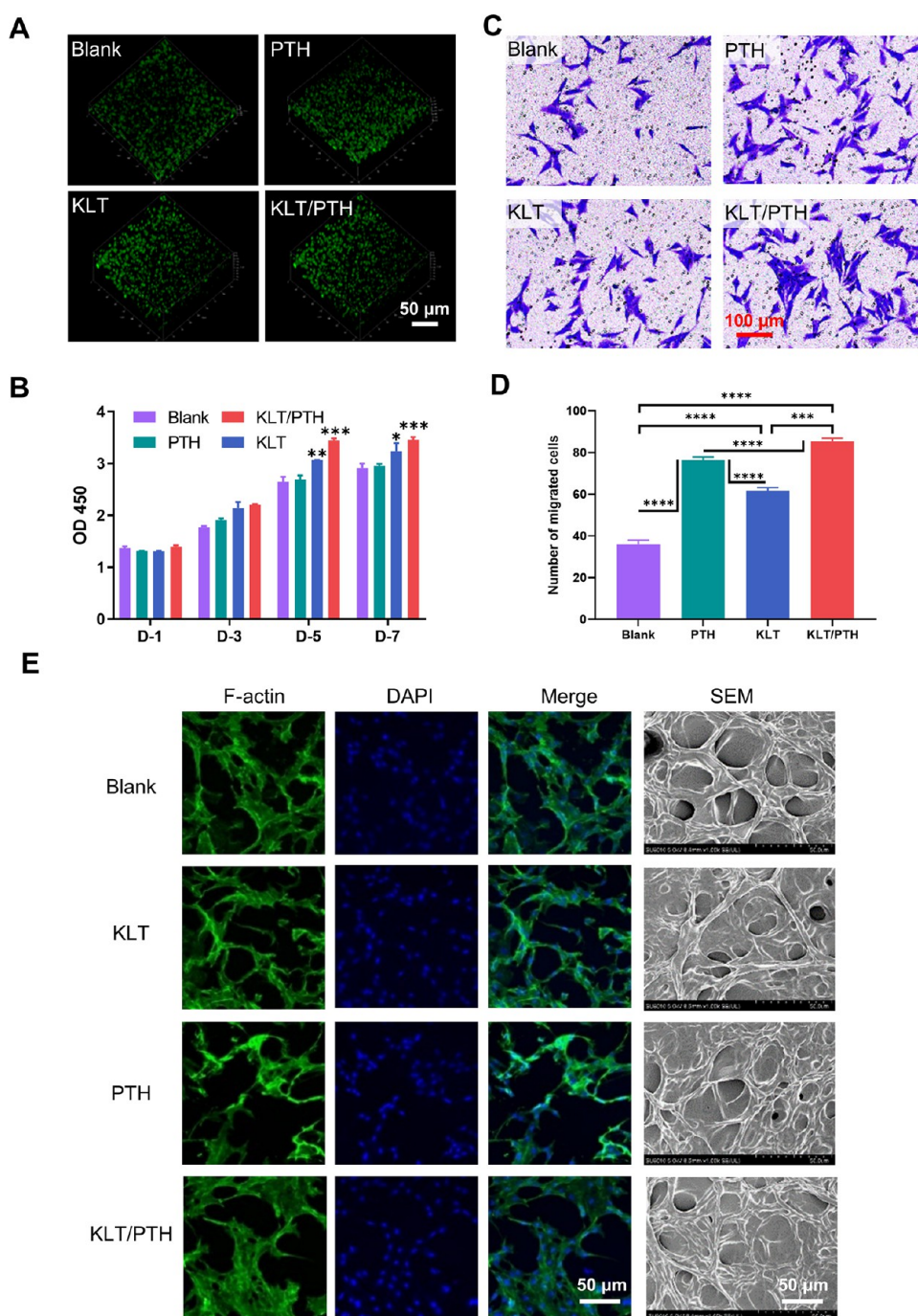


Figure 3. Cytocompatibility of KLT/PTH peptide-functionalized scaffolds. (A) Images of the live/dead assay with BMSCs wrapped in peptide-functionalized hydrogels, the live cells were stained with calcein-AM in green, the dead cells were stained with PI in red, and the BMSCs in peptide-functionalized hydrogels were all stained green (scale bar = 50 μm). (B) KLT/PTH peptide scaffolds increased the proliferation of BMSCs compared with the blank group on day 5 and day 7, as analyzed by a CCK-8 assay. (C) Transwell migration assays of BMSCs with different treatments (scale bar = 100 μm) and (D) quantitative analysis of the number of migrated cells in three regions (1.5 mm \times 1.5 mm) of each group. (E) Fluorescence microscopy images of the cytoskeleton and SEM images of cells on peptide scaffolds (scale bar = 50 μm). Data are represented as mean \pm SD, $n = 3$ per group. (*, $p < 0.05$; **, $p < 0.01$; ***, $p < 0.001$; ****, $p < 0.0001$).

a combination of two types of peptides (Figure 1F) further showed that this gelation strategy might be applied to co-deliver different peptides simultaneously.

Characterization of the Physical Properties of Peptide-Functionalized Hydrogels. As suitable physical properties of hydrogels may enhance the bone regeneration process, we conducted compression tests on the 15% GelNB hydrogels modified with peptides by measuring the compressive stress–

strain curves (Figure 2A). Interestingly, peptide functionalization prior to the crosslinking seemed to impact the hydrogels' physical properties: the incorporation of KLT peptide increased the stiffness, compression modulus, and ultimate stress, while a decrease was observed in the case of using PTH alone (Figures 2B and S4). *In vitro* adhesion properties of the hydrogels were evaluated through gluing tests on fresh porcine skin and measurements of the corresponding adhesion strength using a

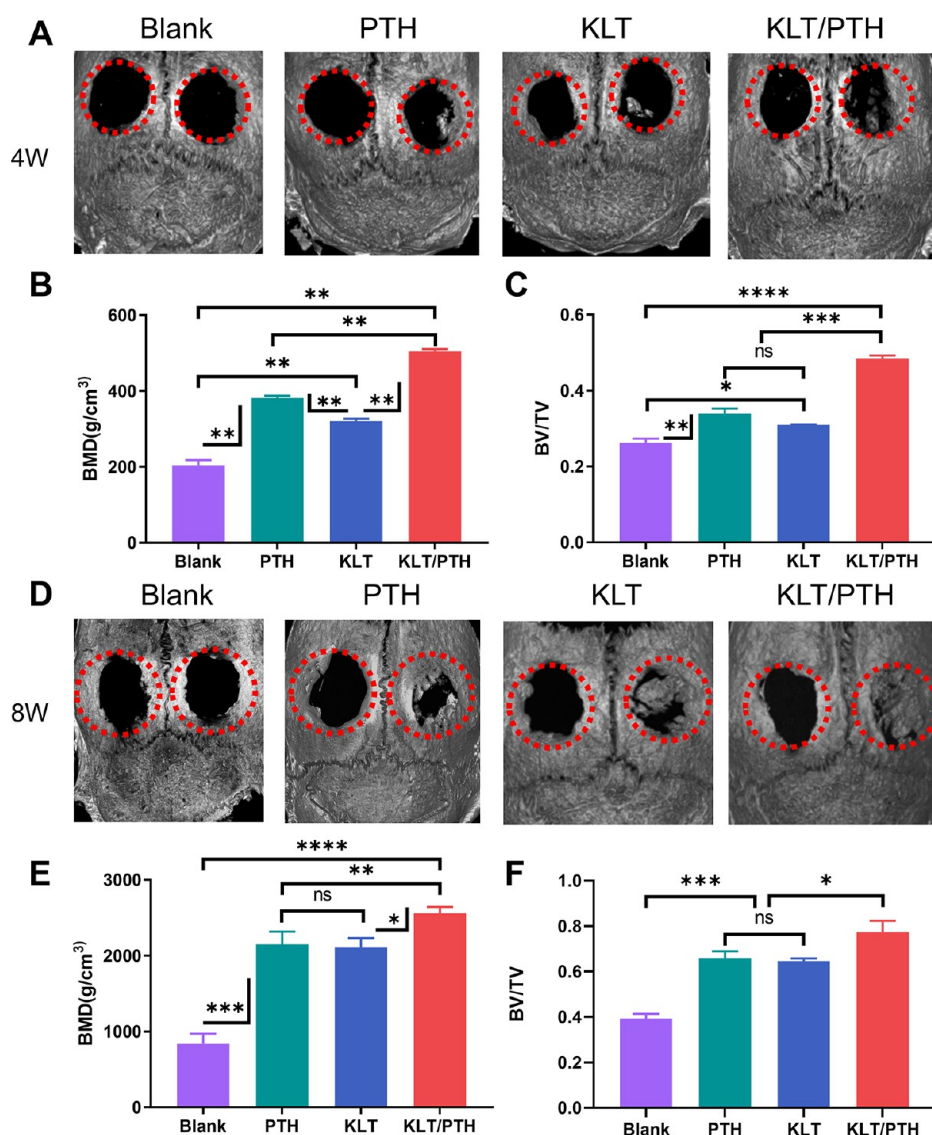


Figure 4. *In vivo* effects of the KLT/PTH peptide-functionalized hydrogels on bone regeneration at 4 and 8 weeks. (A, D) Micro-CT images of the cranial bone defect areas. (B, E) Bone mineral density of defect areas at 4 and 8 weeks. (C, F) Bone volume/total volume of defect areas at 4 and 8 weeks ($n = 3$ per group). (Data are represented as mean \pm SD, *, $p < 0.05$; **, $p < 0.01$; ***, $p < 0.001$; ****, $p < 0.0001$).

mechanical tester (Figure S5B).⁴³ As shown in Figure S5A, two pieces of porcine skin can be firmly attached with all four groups of the hydrogels, which were able to support a weight of 20 g. The adhesion strength of the hydrogels to porcine skin ranged from 8.0 to 12.5 kPa (Figure 2C), similar to a reported GelMA-based hydrogel.³⁴ Scanning electron microscopy (SEM) images of lyophilized hydrogels show that the average pore size of KLT-modified hydrogel (Figure 2D,E), either with or without the PTH peptide (67.1 ± 12.3 or $61.2 \pm 12.9 \mu\text{m}$, respectively), is significantly smaller than that of the unmodified one ($223.5 \pm 36.8 \mu\text{m}$). In contrast, the PTH-modified hydrogel displays a porous structure with an enlarged pore size ($314.9 \pm 32.4 \mu\text{m}$). Considering that the crosslinking density of hydrogel would not be significantly affected by the immobilization of KLT peptide (taken up approx. 5% of all norbornene groups), these results indicate that the installation of varied peptide sequences may have different impacts on the physical properties of hydrogels, presumably through noncovalent interactions with the gelatin peptide chains.

The swelling and enzymatically degrading properties of the prepared hydrogels were also influenced by the incorporated peptides (Figures 2F and S6). After 24 h of incubation in DPBS, all tested hydrogels reached the maximum mass: the swollen mass ratios of the hydrogel without peptide modification (6.5 ± 0.2) and hydrogel containing PTH (6.5 ± 0.2) are significantly higher than that of the ones containing KLT peptide with or without PTH (5.8 ± 0.0 , and 5.9 ± 0.1 , respectively). These results correlate well with the trend that larger pore-sized hydrogels can attract and store more water than the smaller pore-sized ones. Further, the results from incubating the hydrogels with collagenase type II in PBS revealed that the KLT-containing hydrogels degraded at a slower rate than the materials without KLT modification (Figure 2G), where the small-sized pores may impede the accessibility of enzyme to peptides. Moreover, rapid gelation was observed for all gelating materials under dental blue light irradiation (Figure 2H). Oscillatory time sweep tests showed that the elastic modulus (G') and viscous modulus (G'') of the prepared hydrogels were stable as time changed (Figure 2I). Notably, the KLT peptide-

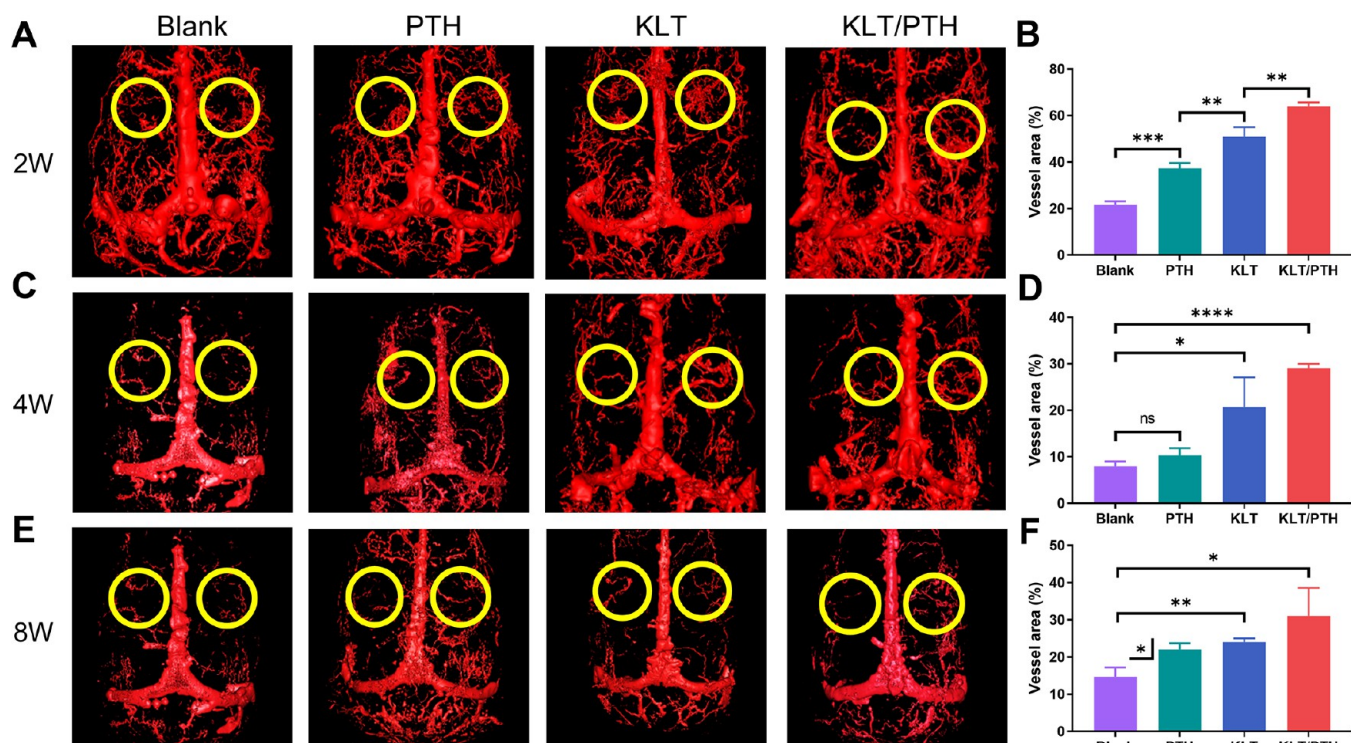


Figure 5. Angiogenic effects of the KLT/PTH peptide-functionalized hydrogels on bone regeneration at 2, 4, and 8 weeks. (A, C, E) Neovascularization micro-CT images of the cranial bone defect areas at 2, 4, and 8 weeks. (B, D, F) Quantitative analysis of neovascularization of the cranial bone defect areas at 2, 4, and 8 weeks ($n = 3$ per group). (Data are represented as mean \pm SD, *, $p < 0.05$; **, $p < 0.01$; ***, $p < 0.001$; ****, $p < 0.0001$).

modified hydrogels display greater G' values than the hydrogel containing only PTH (Figure S7A), suggesting an improved stiffness. In addition, the phase angles of all of the hydrogels were maintained at 0.2 – 1.5° (Figure S7B,C), indicating the highly elastic behavior of the tested hydrogels. Together, these results show that the prepared hydrogels possess suitable physical characteristics as biomaterials for certain medical applications, which prompted us to evaluate their cytocompatibility and biological activities further.

Cytocompatibility of Peptide-Functionalized Hydrogels. To evaluate the cytotoxicity of KLT/PTH peptide-functionalized hydrogels, we conducted live/dead experiments in a bone marrow stromal cell (BMSC) and human umbilical vein endothelial cell (HUVEC) assays, where the cells were wrapped in peptide-functionalized hydrogels and cultured for seven days. As shown in Figures 3A and S8A in the Supporting Information, no obvious cell death was observed, indicating that incorporating peptides into the hydrogel did not influence cell viability. The results from a CCK-8 assay showed a steady increase in cell numbers for the peptide-modified hydrogels over a 7-day culturing period, and the cell numbers of the groups using KLT-containing hydrogel are significantly higher than the groups with hydrogels with PTH modification or without any peptides after 5 days (Figures 3B and S8B). The enhanced cell proliferation may be attributed to the binding of KLT to the receptor on the cell surface, leading to the activation of related signaling pathways.⁴⁴ Further, by conducting a transwell assay to examine the migration ability of BMSCs cultured in the upper compartment of the chamber and different hydrogels in the lower compartment, we discovered that significantly more cells in the KLT/PTH group moved to the lower chamber than those in the other three groups (Figure 3C), which was subsequently

confirmed by quantitative analysis (Figure 3D). Confocal microscopy images of the cell cytoskeleton showed more fluorescent staining for the aligned F-actin fiber in the KLT/PTH group (Figure 3E). The SEM images clearly display that the KLT/PTH-functionalized hydrogel scaffolds are covered with cells in an elongated spindle-like morphology, and more interaction of cells is present. The above results suggested that incorporating the peptide into the hydrogel enhanced the alignment of cell actin fibers, allowing cells to suffer more external mechanical stress. The increased cell adhesion on peptide-functionalized hydrogels might be ascribed to the improved stiffness and the rougher surface of the peptide hydrogels, which are conducive to cell adhesion.⁴⁵

In Vivo Bone Regeneration Effects of Peptide-Functionalized Hydrogels. Critical-sized rat cranial bone defect models were utilized to further evaluate the bone regeneration effects of hydrogels covalently functionalized with KLT and PTH peptides. We seeded the blank, PTH, KLT, and KLT/PTH scaffolds into the right side of the cranial defects, and the left side served as a control without hydrogel. The bone restoration was measured with the micro-CT. The fourth- and eighth-week micro-CT images and quantitative analyses of the bone mineral density (BMD) and BV fractions of the defect areas are shown in Figure 4. Early bone regeneration was evaluated on the fourth week. As shown in Figure 4A, in the blank hydrogel group, there were still large defects, while for the peptide-functionalized hydrogel groups, there was relatively more bone regeneration around the cranial defect. In Figure 4B, a quantitative measurement index for newborn bone growth was conducted using bone mineral density (BMD) and BV/TV. The new bone growth index with BMD and BV/TV was highest in the KLT/PTH group (504.5 ± 4.5 , 0.480 ± 0.005), followed by

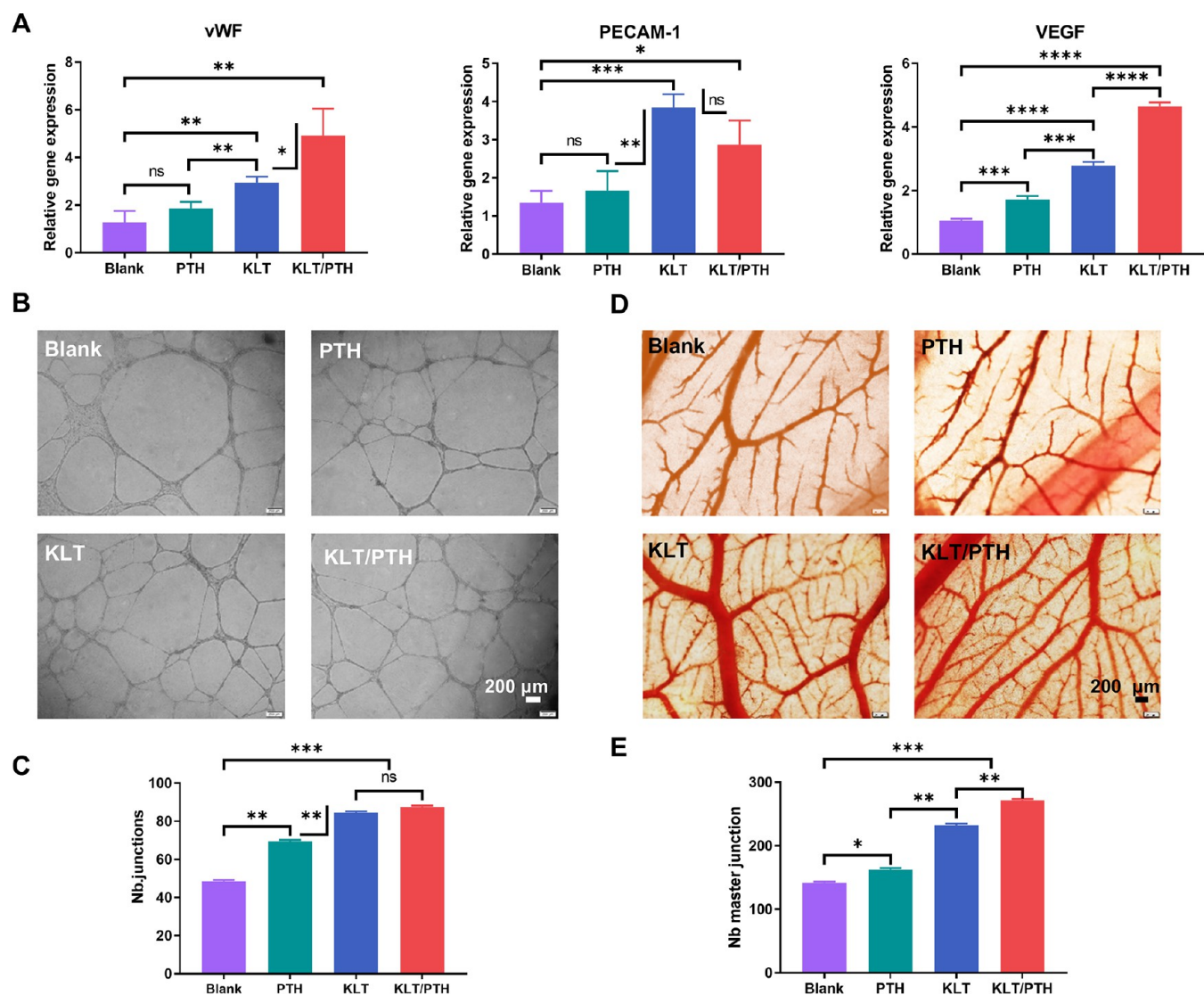


Figure 6. Gene expression and angiogenic effect of KLT/PTH peptide. (A) The proangiogenic gene expression of vWF, PECAW, and VEGF of HUVECs; (B) tube formation assays with HUVECs were performed and observed after 8 h; (C) quantitative analysis of the master junctions; (D) formed blood vessels on the CAM were photographed after fixation; and (E) number of newly formed microvessels were quantified ($n = 3$ per group). (Data are represented as mean \pm SD, *, $p < 0.05$; **, $p < 0.01$; ***, $p < 0.001$; ****, $p < 0.0001$).

the PTH (382.0 ± 3.9 , 0.340 ± 0.009) and KLT (321.0 ± 4.0 , 0.309 ± 0.001) groups, which showed better results than the group filled only with the hydrogel scaffold (204.0 ± 9.5 , 0.262 ± 0.008) ($p < 0.01$). At 4 weeks postoperatively, new bone formation was evident in the KLT/PTH group (Figure 4C). Quantitative analysis showed the same trend for the increase in BMD and BV/TV at 8 weeks after surgery. In detail, the most bone regeneration of BMD and BV/TV was observed in KLT/PTH group (2559 ± 86 , 0.773 ± 0.029), which was significantly higher than the PTH (2151 ± 168 , 0.660 ± 0.017) and KLT (2111 ± 123 , 0.647 ± 0.007) groups. All three peptide-functionalized groups showed a significant regenerative effect compared with the blank group (838 ± 132 , 0.393 ± 0.012) ($p < 0.01$).

HE and Masson's trichrome staining further histologically confirmed the formation and maturity of new bone (Figures S9 and S10). Consistent with the micro-CT results, staining of the cranial bone tissues showed that all hydrogel groups were undergoing bone restoration to a certain extent. As shown in the HE images, no inflammatory reaction or necrosis was observed

in any of the groups. Four weeks after surgery, fibrous connective tissue was mainly observed in the blank group. A small amount of new bone tissue was seen in the blank group, and new bone appeared in the PTH and KLT groups, especially the KLT/PTH group. Masson's trichrome staining revealed that collagen fibers, calcified tissue, and cartilage were stained blue; muscle fibers and cellulose were stained red; and nuclei were stained blue-black. As shown in Figure S9B, scarce collagen fibers and calcified tissues developed at the defect site in the blank group at 4 weeks. In the PTH and KLT groups, there were more collagen fibers and ossification tissues than in the blank group, while the KLT/PTH group showed the most significant calcified tissues. At 8 weeks postoperatively (Figure S10B), bone regeneration was obvious, and the calcified tissues in the KLT/PTH group were significantly greater than those in the other three groups. Immunohistochemical staining of OCN, which is a bone tissue-specific protein, was also conducted to obtain further insights into the effect of peptide covalently functionalized hydrogels on bone regeneration *in vivo* (Figures S9D and S10D). At both 4 and 8 weeks after the surgery, all three groups functionalized

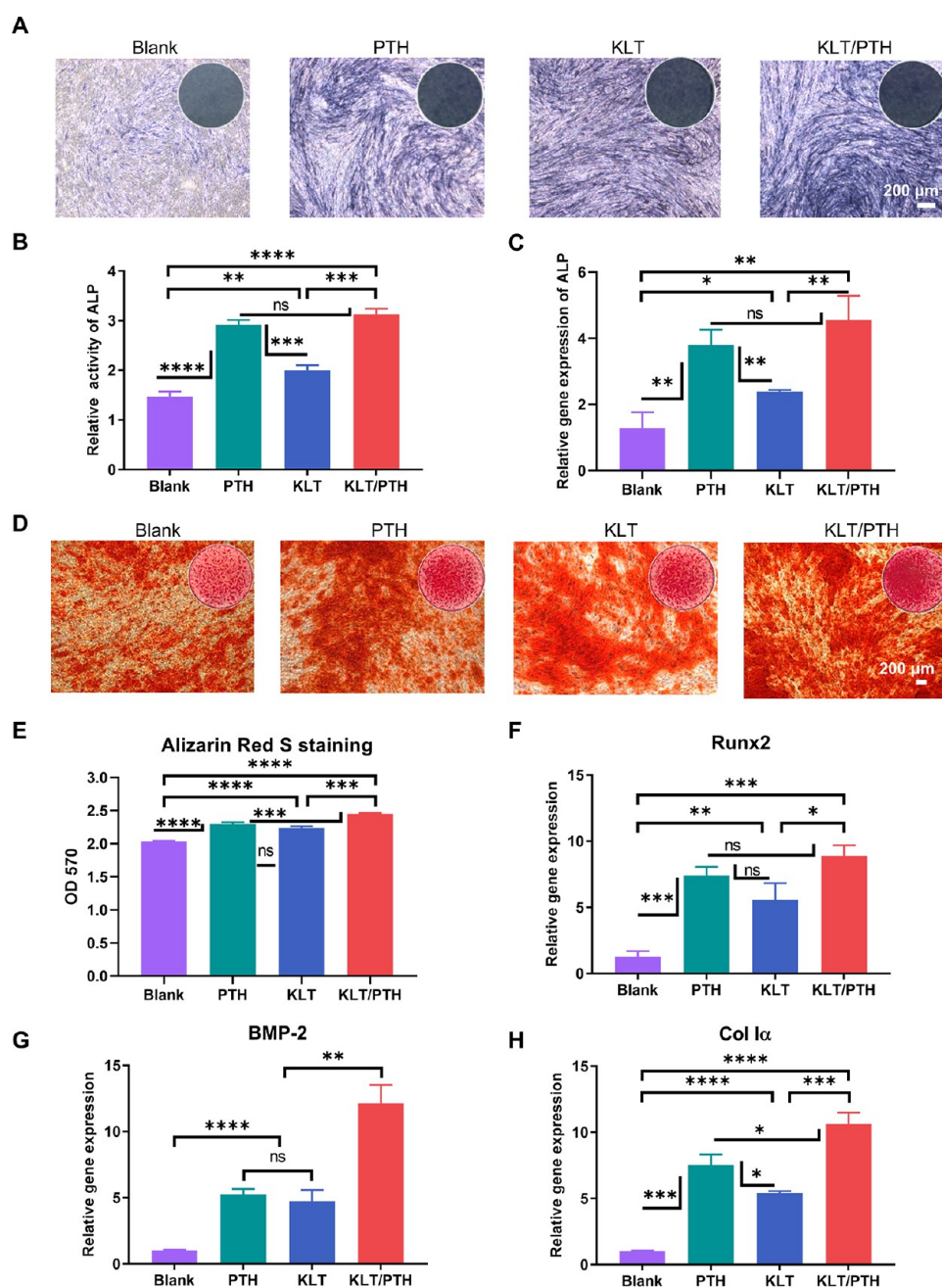


Figure 7. Effects of KLT/PTH peptide on the osteogenic differentiation of BMSCs. (A) ALP staining, (B) ALP activity, (C) RT-PCR analysis of ALP, (D) Alizarin red staining, (E) quantification of mineral deposits, and (F–H) osteogenic gene expression (Runx2, BMP2, and Col 1 α) in BMSCs. The results confirmed that the PTH, KLT, and KLT/PTH combination promoted osteogenic differentiation of BMSCs and that synergistic PHT and KLT showed the most significant upregulation effect ($n = 3$ per group). (Data are represented as mean \pm SD, *, $p < 0.05$; **, $p < 0.01$; ***, $p < 0.001$; ****, $p < 0.0001$).

with bioactive peptides exhibited positive staining of OCN. These results indicated that PTH and KLT covalently functionalized hydrogel scaffolds exerted a positive effect on bone regeneration.

Neovascularization formation is an important part of bone regeneration. With adequate blood vessel regeneration, more oxygen and nutrients could be transported. To confirm blood vessel growth at the cranial defect site, vascular perfusion was performed, and neovascularization in the defect area was observed clearly by micro-CT. The 3D construction images are shown in Figure 5. The results showed that compared to the blank group, the peptide-incorporated groups exhibited

strikingly enhanced angiogenesis, and the KLT/PTH group showed more blood vessel growth than the other three groups at 2, 4, and 8 weeks. Quantification of the new capillary formation was consistent with the trend. Platelet endothelial cell adhesion molecule (PECAM-1), also known as cluster of differentiation 31 (CD31), can help to evaluate the degree of angiogenesis. Immunohistochemical staining of CD31 was conducted (Figures S9C and S10C). At 4 weeks after the surgery, the immunohistochemistry staining results indicated more abundant areas of CD31 cells in the KLT/PTH group than in the other three groups. All three groups exhibited positive staining of CD31 at 8 weeks postoperation. These findings suggested that

the combined treatment of PTH and KLT stimulated angiogenesis, thus potentially improving calvarial bone formation through neovascularization mechanisms.

Mechanistic Insight into the Potential Synergistic Effects of KLT/PTH Peptides. As we have demonstrated that the combination of KLT and PTH in hydrogel showed the best *in vivo* regenerative efficacy, we set out to evaluate the angiogenic effects of KLT/PTH peptides, using human umbilical vein endothelial cells (HUVECs) in a capillary tube formation assay and a chick embryo chorioallantoic membrane (CAM) assay. First, we cultured HUVECs with peptides for seven days and detected the mRNA expression of proangiogenic genes. Real-time PCR (RT-PCR) results (Figure 6A) showed that the KLT peptide alone significantly upregulated the mRNA levels of VEGF, PECAW, and vWF compared to the blank group. Remarkably, with the combination of KLT and PTH, VEGF and vWF expression achieved the highest level, suggesting that the combination of PTH and KLT may synergistically promote the angiogenic ability of HUVECs. Meanwhile, the capillary tube formation assay indicated better tube formation performance (characterized by a greater total tube length and complete tubular structure) in the KLT/PTH group than in the PTH, KLT, and blank groups (Figure 6B). The tube formation counts (Figure 6C) verified the above-mentioned results. Moreover, the angiogenic efficacy of the peptides was assessed by a CAM assay. Many microvessels were observed for the KLT peptide alone or combined with PTH (Figure 6D), and the quantitative data for the major number of master junctions of vessels proved that the KLT/PTH group significantly promoted the new formation of blood vessels compared to the blank group (Figure 6E). These results indicated that the KLT peptide effectively promoted the angiogenesis efficacy of HUVECs. VEGF has been reported as a potent growth factor for angiogenesis,⁴⁶ and the VEGF mimetic peptide KLT showed the same biological properties in the present study. Furthermore, we found that the KLT/PTH combination showed better angiogenic efficacy than KLT alone.

Next, we evaluated the osteogenic differentiation ability of the KLT/PTH combination by measuring the alkaline phosphatase (ALP) expression level and conducting Alizarin red staining (ARS) and gene expression tests. To begin with, ALP, an early osteogenic marker for osteogenic differentiation, was measured to evaluate the osteogenic ability of the peptides by both staining and mRNA expression. As shown in Figure 7, either PTH or KLT peptide alone, or a combination of the two, exhibited more dark staining and higher ALP protein expression compared to the blank group. The mRNA expression of ALP was in accord with the staining outcomes (Figure 7C). The combination of KLT/PTH significantly increased ALP mRNA expression 4.2-fold compared with the blank group. After culturing for 14 days, calcium deposition was detected with Alizarin red staining (ARS) to reveal the late osteogenic differentiation ability (Figure 7D). The stained nodules produced by the KLT/PTH combination were the most abundant compared to the blank group, or PTH or KLT alone. The quantification of the mineral deposits was consistent with the ARS results (Figure 7E) and confirmed by the mRNA expression levels of gene markers related to bone formation, including Runx2, BMP-2, and Col 1 α (Figure 7F–H). While we have observed that PTH alone exhibited an apparent osteogenic effect, the above-mentioned results revealed that the PTH and KLT peptide combination promoted osteogenic differentiation better than the PTH peptide alone. A previous study reported that VEGF led to

increased osteogenesis through activation of Akt signaling,⁴⁷ while another study found that PTH could activate the antiapoptotic signaling pathway of the phosphoinositide 3-kinase-Akt-Bad cascade.⁴⁸ Therefore, it was reasonable that the combined use of PTH and KLT might synergistically amplify Akt signaling to promote osteogenesis.

In our *in vivo* study on rat models, the KLT/PTH hydrogel exhibited a remarkable regenerative efficacy of $77.3 \pm 5.0\%$ BV/TV in 8 weeks, exceeding all of the previously reported PTH-loaded hydrogel systems.^{49–51} Based on the above *in vitro* tests, we reason that the excellent regenerative ability induced by the KLT/PTH hydrogel may be attributed to the following aspects. At the early stage of bone regeneration, with the combinational treatment of KLT/PTH, a large number of endothelial cells could be recruited to the defect site, forming new blood vessels. As a result, more oxygen, nutrients, ions, and BMSCs could be transported. Furthermore, the combinational stimulation of KLT/PTH significantly enhanced the attachment of stem cells to the hydrogel. Finally, the upregulated expression of MMPs at the defect site⁵² could degrade the hydrogel scaffold, achieving the continuous release of PTH(1–34) and KLT peptide to maintain the local environment for stem cell recruitment and osteogenic differentiation. This kind of virtuous cycle eventually leads to efficient bone regeneration.

CONCLUSIONS

In summary, we have demonstrated that the combined utilization of the peptides KLT and PTH(1–34) could synergistically promote both *in vitro* and *in vivo* angiogenic and osteogenic processes. Based on a norbornene-functionalized gelatin scaffold, we have shown that the covalent incorporation of active peptide component and simultaneous hydrogel curation could be accomplished within seconds under dental blue light irradiation, which provided favorable convenience and safety that meets the clinical demands. In addition, covalently installed KLT and PTH peptides in hydrogel facilitate slow-release, benefiting the usually long course of bone regeneration. The KLT/PTH-functionalized hydrogel performed excellently in a rat cranial defect model, suggesting that co-delivery of an angiogenic VEGF mimetic peptide and an osteogenic factor may be of excellent prospects in the application of bone tissue regeneration. We believe that further optimization on this hydrogel system, such as incorporating other structural components (e.g., nanohydroxyapatite or ceramic) to increase its mechanical and osteoinductive properties, may be highly useful in producing more effective biomaterials for therapeutic use.

ASSOCIATED CONTENT

Supporting Information

The Supporting Information is available free of charge at <https://pubs.acs.org/doi/10.1021/acsami.2c06159>.

Primers for reverse-transcription polymerase, receptor binding activity for the PTH(1–34) analogues, ¹H NMR spectrum of gelatin and GelNB, schematics of a plausible mechanism for the photoinduced thiol-norbornene reaction, ultimate stress from compression tests, *in vitro* adhesion properties of the hydrogels, mass swelling ratio of the hydrogels, rheological properties of the hydrogels, cytocompatibility in human umbilical vein endothelial cells, histological images of bone defect areas at 4 weeks, histological images of bone defect areas at 8 weeks,

HPLC-MS analysis of PTH[NiE8,18]₁₋₃₄, HPLC-MS analysis of GCG-PTH[NiE8,18]₁₋₃₄, HPLC-MS analysis of PTH[NiE8,18]₁₋₃₄-GCG, HPLC-MS analysis of KLT peptide, HPLC-MS analysis of GCG-KLT peptide, and HPLC-MS analysis of MMP-degradable peptide linker (PDF)

AUTHOR INFORMATION

Corresponding Authors

Yuguang Wang – National Engineering Laboratory for Digital and Material Technology of Stomatology, National Clinical Research Center for Oral Diseases, Beijing Key Laboratory of Digital Stomatology, and Department of Pediatric Dentistry, Peking University School and Hospital of Stomatology, Beijing 100081, China; Email: young13doctor@163.com

Suwei Dong – State Key Laboratory of Natural and Biomimetic Drugs, Chemical Biology Center, and School of Pharmaceutical Sciences, Peking University, Beijing 100191, China; orcid.org/0000-0002-2648-4344; Email: dongsw@pku.edu.cn

Authors

Guiyan Wang – National Engineering Laboratory for Digital and Material Technology of Stomatology, National Clinical Research Center for Oral Diseases, Beijing Key Laboratory of Digital Stomatology, and Department of Pediatric Dentistry, Peking University School and Hospital of Stomatology, Beijing 100081, China

Ning Yuan – State Key Laboratory of Natural and Biomimetic Drugs, Chemical Biology Center, and School of Pharmaceutical Sciences, Peking University, Beijing 100191, China

Ningyu Li – Department of Oral Comprehensive Treatment, Jilin University School and Hospital of Stomatology, Changchun 130021, China

Qijia Wei – State Key Laboratory of Natural and Biomimetic Drugs, Chemical Biology Center, and School of Pharmaceutical Sciences, Peking University, Beijing 100191, China

Yuping Qian – Department of Prosthodontics, Jilin University School and Hospital of Stomatology, Changchun 130021, China

Jun Zhang – State Key Laboratory of Natural and Biomimetic Drugs, Chemical Biology Center, and School of Pharmaceutical Sciences, Peking University, Beijing 100191, China

Man Qin – National Engineering Laboratory for Digital and Material Technology of Stomatology, National Clinical Research Center for Oral Diseases, Beijing Key Laboratory of Digital Stomatology, and Department of Pediatric Dentistry, Peking University School and Hospital of Stomatology, Beijing 100081, China

Complete contact information is available at:
<https://pubs.acs.org/10.1021/acsami.2c06159>

Author Contributions

¹G.W. and N.Y. contributed equally.

Notes

The authors declare no competing financial interest.

ACKNOWLEDGMENTS

The authors are grateful for financial support from the Beijing National Science Foundation (JQ18024), the National Natural Science Foundation of China (51972003), and Intergovernmental International Cooperation Project of the Ministry of

Science and Technology (2018YFE0192500) for their support. They thank Dr. Wei Bai (Peking University School and Hospital of Stomatology) for assistance with mechanical tests.

REFERENCES

- (1) Zouhary, K. J. Bone Graft Harvesting from Distant Sites: Concepts and Techniques. *Oral Maxillofac. Surg. Clin. North Am.* **2010**, *22*, 301–316.
- (2) Gaharwar, A. K.; Singh, I.; Khademhosseini, A. Engineered Biomaterials for In Situ Tissue Regeneration. *Nat. Rev. Mater.* **2020**, *5*, 686–705.
- (3) O'Brien, F. J. Biomaterials & Scaffolds for Tissue Engineering. *Mater. Today* **2011**, *14*, 88–95.
- (4) Furth, M. E.; Atala, A.; Van Dyke, M. E. Smart Biomaterials Design for Tissue Engineering and Regenerative Medicine. *Biomaterials* **2007**, *28*, 5068–5073.
- (5) McKay, W. F.; Peckham, S. M.; Badura, J. M. A Comprehensive Clinical Review of Recombinant Human Bone Morphogenetic Protein-2 (INFUSE Bone Graft). *Int. Orthop.* **2007**, *31*, 729–734.
- (6) Yu, X.; Tang, X.; Gohil, S. V.; Laurencin, C. T. Biomaterials for Bone Regenerative Engineering. *Adv. Healthcare Mater.* **2015**, *4*, 1268–1285.
- (7) Liao, J.; Wu, S.; Li, K.; Fan, Y.; Dunne, N.; Li, X. Peptide-Modified Bone Repair Materials: Factors Influencing Osteogenic Activity. *J. Biomed. Mater. Res., Part A* **2019**, *107*, 1491–1512.
- (8) Li, R.; Sun, Y.; Cai, Z.; Li, Y.; Sun, J.; Bi, W.; Yang, F.; Zhou, Q.; Ye, T.; Yu, Y. Highly Bioactive Peptide-HA Photo-Crosslinking Hydrogel for Sustained Promoting Bone Regeneration. *Chem. Eng. J.* **2021**, *415*, No. 129015.
- (9) Li, X.; Sun, Q.; Li, Q.; Kawazoe, N.; Chen, G. Functional Hydrogels with Tunable Structures and Properties for Tissue Engineering Applications. *Front. Chem.* **2018**, *6*, No. 499.
- (10) Zhang, Y.; Yu, T.; Peng, L.; Sun, Q.; Wei, Y.; Han, B. Advancements in Hydrogel-Based Drug Sustained Release Systems for Bone Tissue Engineering. *Front. Pharmacol.* **2020**, *11*, No. 622.
- (11) Qiao, Y.; Liu, X.; Zhou, X.; Zhang, H.; Zhang, W.; Xiao, W.; Pan, G.; Cui, W.; Santos, H. A.; Shi, Q. Gelatin Templated Polypeptide Co-Cross-Linked Hydrogel for Bone Regeneration. *Adv. Healthcare Mater.* **2020**, *9*, No. e1901239.
- (12) Li, R.; Lin, S.; Zhu, M.; Deng, Y.; Chen, X.; Wei, K.; Xu, J.; Li, G.; Bian, L. Synthetic Presentation of Noncanonical Wnt5a Motif Promotes Mechanosensing-Dependent Differentiation of Stem Cells and Regeneration. *Sci. Adv.* **2019**, *5*, No. eaaw3896.
- (13) Park, S. H.; Park, J. Y.; Ji, Y. B.; Ju, H. J.; Min, B. H.; Kim, M. S. An Injectable Click-Crosslinked Hyaluronic Acid Hydrogel Modified with a BMP-2 Mimetic Peptide as a Bone Tissue Engineering Scaffold. *Acta Biomater.* **2020**, *117*, 108–120.
- (14) Dimitriou, R.; Jones, E.; McGonagle, D.; Giannoudis, P. V. Bone Regeneration: Current Concepts and Future Directions. *BMC Med.* **2011**, *9*, No. 66.
- (15) Majidinia, M.; Sadeghpour, A.; Yousefi, B. The Roles of Signaling Pathways in Bone Repair and Regeneration. *J. Cell. Physiol.* **2018**, *233*, 2937–2948.
- (16) D'Andrea, L. D.; Iaccarino, G.; Fattorusso, R.; Sorriento, D.; Carannante, C.; Capasso, D.; Trimarco, B.; Pedone, C. Targeting Angiogenesis: Structural Characterization and Biological Properties of a De Novo Engineered VEGF Mimicking Peptide. *Proc. Natl. Acad. Sci. U.S.A.* **2005**, *102*, 14215–14220.
- (17) Lu, J.; Guan, F.; Cui, F.; Sun, X.; Zhao, L.; Wang, Y.; Wang, X. Enhanced Angiogenesis by the Hyaluronic Acid Hydrogels Immobilized with a VEGF Mimetic Peptide in a Traumatic Brain Injury Model in Rats. *Regen. Biomater.* **2019**, *6*, 325–334.
- (18) Canalis, E.; Giustina, A.; Bilezikian, J. P. Mechanisms of Anabolic Therapies for Osteoporosis. *N. Engl. J. Med.* **2007**, *357*, 905–916.
- (19) Carano, R. A. D.; Filvaroff, E. H. Angiogenesis and Bone Repair. *Drug Discovery Today* **2003**, *8*, 980–989.

- (20) Chiu, L. L.; Radisic, M. Scaffolds with Covalently Immobilized VEGF and Angiopoietin-1 for Vascularization of Engineered Tissues. *Biomaterials* **2010**, *31*, 226–241.
- (21) Gregoritzka, M.; Messmann, V.; Goepferich, A. M.; Brandl, F. P. Design of Hydrogels for Delayed Antibody Release Utilizing Hydrophobic Association and Diels-Alder Chemistry in Tandem. *J. Mater. Chem. B* **2016**, *4*, 3398–3408.
- (22) Nguyen, M. K.; Huynh, C. T.; Gilewski, A.; Wilner, S. E.; Maier, K. E.; Kwon, N.; Levy, M.; Alsborg, E. Covalently Tethering siRNA to Hydrogels for Localized, Controlled Release and Gene Silencing. *Sci. Adv.* **2019**, *5*, No. eaax0801.
- (23) Cai, Z.; Wei, Q.; Li, X.; Luan, Y.; Dong, S. Chemical Syntheses and Biological Evaluation of CXCL14 and Its Site-Selectively Modified Methionine Sulfoxide-Containing Derivatives. *J. Org. Chem.* **2020**, *85*, 1740–1747.
- (24) Van Hoorick, J.; Gruber, P.; Markovic, M.; Rollot, M.; Graulus, G. J.; Vagenende, M.; Tromayer, M.; Van Erps, J.; Thienpont, H.; Martins, J. C.; Baudis, S.; Ovsianikov, A.; Dubruel, P.; Van Vlierbergh, S. Highly Reactive Thiol-Norbornene Photo-Click Hydrogels: Toward Improved Processability. *Macromol. Rapid Commun.* **2018**, *39*, No. e1800181.
- (25) Göckler, T.; Haase, S.; Kempter, X.; Pfister, R.; Maciel, B. R.; Grimm, A.; Molitor, T.; Willenbacher, N.; Schepers, U. Tuning Superfast Curing Thiol-Norbornene-Functionalized Gelatin Hydrogels for 3D Bioprinting. *Adv. Healthcare Mater.* **2021**, *10*, No. e2100206.
- (26) Kumar, V. A.; Taylor, N. L.; Shi, S.; Wang, B. K.; Jalan, A. A.; Kang, M. K.; Wickremasinghe, N. C.; Hartgerink, J. D. Highly Angiogenic Peptide Nanofibers. *ACS Nano* **2015**, *9*, 860–868.
- (27) Ma, X.; Agas, A.; Siddiqui, Z.; Kim, K.; Iglesias-Montoro, P.; Kalluru, J.; Kumar, V.; Haorah, J. Angiogenic Peptide Hydrogels For Treatment of Traumatic Brain Injury. *Bioact. Mater.* **2020**, *5*, 124–132.
- (28) Arrighi, I.; Mark, S.; Alvisi, M.; von Rechenberg, B.; Hubbell, J. A.; Schense, J. C. Bone Healing Induced by Local Delivery of an Engineered Parathyroid Hormone Prodrug. *Biomaterials* **2009**, *30*, 1763–1771.
- (29) Jung, R. E.; Cochran, D. L.; Domken, O.; Seibl, R.; Jones, A. A.; Buser, D.; Hammerle, C. H. F. The Effect of Matrix Bound Parathyroid Hormone on Bone Regeneration. *Clin. Oral Implants Res.* **2007**, *18*, 319–325.
- (30) Valderrama, P.; Jung, R. E.; Thoma, D. S.; Jones, A. A.; Cochran, D. L. Evaluation of Parathyroid Hormone Bound to a Synthetic Matrix for Guided Bone Regeneration Around Dental Implants: A Histomorphometric Study in Dogs. *J. Periodontol.* **2010**, *81*, 737–747.
- (31) Dong, S.; Shang, S.; Li, J.; Tan, Z.; Dean, T.; Maeda, A.; Gardella, T. J.; Danishefsky, S. J. Engineering of Therapeutic Polypeptides Through Chemical Synthesis: Early Lessons From Human Parathyroid Hormone and Analogues. *J. Am. Chem. Soc.* **2012**, *134*, 15122–15129.
- (32) Bastepe, M.; Turan, S.; He, Q. Heterotrimeric G Proteins in the Control of Parathyroid Hormone Actions. *J. Mol. Endocrinol.* **2017**, *58*, R203–R224.
- (33) Clark, L. J.; Krieger, J.; White, A. D.; Bondarenko, V.; Lei, S.; Fang, F.; Lee, J. Y.; Doruker, P.; Bottke, T.; Jean-Alphonse, F.; Tang, P.; Gardella, T. J.; Xiao, K.; Sutkeviciute, I.; Coin, I.; Bahar, I.; Vilardaga, J. P. Allosteric Interactions in the Parathyroid Hormone GPCR-Arrestin Complex Formation. *Nat. Chem. Biol.* **2020**, *16*, 1096–1104.
- (34) Li, F.; Truong, V. X.; Thissen, H.; Frith, J. E.; Forsythe, J. S. Microfluidic Encapsulation of Human Mesenchymal Stem Cells for Articular Cartilage Tissue Regeneration. *ACS Appl. Mater. Interfaces* **2017**, *9*, 8589–8601.
- (35) Shirzaei Sani, E.; Lara, R. P.; Aldawood, Z.; Bassir, S. H.; Nguyen, D.; Kantarci, A.; Intini, G.; Annabi, N. An Antimicrobial Dental Light Curable Bioadhesive Hydrogel for Treatment of Peri-Implant Diseases. *Matter* **2019**, *1*, 926–944.
- (36) Shirzaei Sani, E.; Kheirkhah, A.; Rana, D.; Sun, Z.; Foulsham, W.; Sheikhi, A.; Khademhosseini, A.; Dana, R.; Annabi, N. Sutureless Repair of Corneal Injuries Using Naturally Derived Bioadhesive Hydrogels. *Sci. Adv.* **2019**, *5*, No. eaav1281.
- (37) Noshadi, I.; Hong, S.; Sullivan, K. E.; Shirzaei Sani, E.; Portillo-Lara, R.; Tamayol, A.; Shin, S. R.; Gao, A. E.; Stoppel, W. L.; Black, L. D., III; Khademhosseini, A.; Annabi, N. In Vitro and In Vivo Analysis of Visible Light Crosslinkable Gelatin Methacryloyl (GelMA) Hydrogels. *Biomater. Sci.* **2017**, *5*, 2093–2105.
- (38) Shih, H.; Lin, C.-C. Visible-Light-Mediated Thiol-Ene Hydrogelation Using Eosin-Y as the Only Photoinitiator. *Macromol. Rapid Commun.* **2013**, *34*, 269–273.
- (39) Carthew, J.; Donderwinkel, I.; Shrestha, S.; Truong, V. X.; Forsythe, J. S.; Frith, J. E. In Situ miRNA Delivery from a Hydrogel Promotes Osteogenesis of Encapsulated Mesenchymal Stromal Cells. *Acta Biomater.* **2020**, *101*, 249–261.
- (40) Hu, W.; Wang, Z.; Xiao, Y.; Zhang, S.; Wang, J. Advances in Crosslinking Strategies of Biomedical Hydrogels. *Biomater. Sci.* **2019**, *7*, 843–855.
- (41) Patterson, J.; Hubbell, J. A. Enhanced Proteolytic Degradation of Molecularly Engineered PEG Hydrogels in Response to MMP-1 and MMP-2. *Biomaterials* **2010**, *31*, 7836–7845.
- (42) Van Hove, A. H.; Burke, K.; Antonienko, E.; Brown, E.; Benoit, D. S. W. Enzymatically-Responsive Pro-Angiogenic Peptide-Releasing Poly(Ethylene Glycol) Hydrogels Promote Vascularization In Vivo. *J. Control. Release* **2015**, *217*, 191–201.
- (43) Chen, S.; Xie, J.; Liu, J.; Huang, X.; Wang, C. Transparent, Highly-Stretchable, Adhesive, and Ionic Conductive Composite Hydrogel for Biomimetic Skin. *J. Mater. Sci.* **2021**, *56*, 2725–2737.
- (44) Nilsson, M.; Heymach, J. V. Vascular Endothelial Growth Factor (VEGF) Pathway. *J. Thorac. Oncol.* **2006**, *1*, 768–770.
- (45) Yang, J.; Bai, R.; Chen, B.; Suo, Z. Hydrogel Adhesion: A Supramolecular Synergy of Chemistry, Topology, and Mechanics. *Adv. Funct. Mater.* **2019**, *30*, No. 1901693.
- (46) Tang, W.; Yu, Y.; Wang, J.; Liu, H.; Pan, H.; Wang, G.; Liu, C. Enhancement and Orchestration of Osteogenesis and Angiogenesis by a Dual-Modular Design of Growth Factors Delivery Scaffolds and 26SCS Decoration. *Biomaterials* **2020**, *232*, No. 119645.
- (47) Lu, W.; Xu, W.; Li, J.; Chen, Y.; Pan, Y.; Wu, B. Effects of Vascular Endothelial Growth Factor and Insulin Growth Factor 1 on Proliferation, Migration, Osteogenesis and Vascularization of Human Carious Dental Pulp Stem Cells. *Mol. Med. Rep.* **2019**, *20*, 3924–3932.
- (48) Yamamoto, T.; Kambe, F.; Cao, X.; Lu, X.; Ishiguro, N.; Seo, H. Parathyroid Hormone Activates Phosphoinositide 3-Kinase-Akt-Bad Cascade in Osteoblast-Like Cells. *Bone* **2007**, *40*, 354–359.
- (49) Dang, M.; Koh, A. J.; Jin, X.; McCauley, L. K.; Ma, P. X. Local Pulsatile PTH Delivery Regenerates Bone Defects via Enhanced Bone Remodeling in a Cell-Free Scaffold. *Biomaterials* **2017**, *114*, 1–9.
- (50) Zou, Z.; Wang, L.; Zhou, Z.; Sun, Q.; Liu, D.; Chen, Y.; Hu, H.; Cai, Y.; Lin, S.; Yu, Z.; Tan, B.; Guo, W.; Ling, Z.; Zou, X. Simultaneous Incorporation of PTH(1-34) and Nano-Hydroxyapatite into Chitosan/Alginate Hydrogels for Efficient Bone Regeneration. *Bioact. Mater.* **2021**, *6*, 1839–1851.
- (51) Kuang, L.; Huang, J.; Liu, Y.; Li, X.; Yuan, Y.; Liu, C. Injectable Hydrogel with NIR Light-Responsive, Dual-Mode PTH Release for Osteoregeneration in Osteoporosis. *Adv. Funct. Mater.* **2021**, *31*, No. 2105383.
- (52) Liang, H. P. H.; Xu, J.; Xue, M.; Jackson, C. Matrix Metalloproteinases in Bone Development and Pathology: Current Knowledge and Potential Clinical Utility. *Metalloproteinases Med.* **2016**, *3*, 93–102.